SUPPLEMENTARY MATERIAL

Anti-inflammatory effect of methoxyflavonoids from *Chiliadenus montanus* (*Jasonia montana)* growing in Egypt

Eman S. Habib[1], Eman El-Bsoumy[2], Amany K. Ibrahim[1], Mohamed A. Helal[3,4]

Mohammed A. El-Magd[5]* and Safwat A. Ahmed[1*]

[1]*Department of Pharmacognosy, Faculty of Pharmacy, Suez Canal University, Ismailia, Egypt 41522;* [2]*Department of Pharmacognosy, College of Pharmacy, Arab Academy for Science, Technology and Maritime Transport;* [3]*Biomedical Sciences Program, University of Science and Technology, Zewail City of Science and Technology, October Gardens, 6th of October, Giza 12587;* [4]*Department of Medicinal Chemistry, Faculty of Pharmacy, Suez Canal University, Ismailia, Egypt 41522;* [5]*Department of Anatomy, Faculty of Veterinary Medicine, Kafrelsheikh University, Egypt.*

*Corresponding authors: Email: Safwat A. Ahmed: safwat_aa@yahoo.com

and Mohammed A. El-Magd: mohamed.abouelmagd@vet.kfs.edu.eg; ORCID: https://orcid.org/0000-0002-3314-9202

Short title " *Chiliadenus montanus* anti-inflammatory effect"

Anti-inflammatory effect of methoxyflavonoids from *Chiliadenus montanus* (*Jasonia montana)* growing in Egypt

ABSTRACT

Chiliadenus montanus is a medicinal plant that grows in Sinai Peninsula in Egypt. Phytochemical investigation of *C. montanus* methanolic extract led to the isolation of five methoxy flavonoids; Chrysosplenol-D **(1) ,** 5,7,4'-trihydroxy- 3,3'-dimethoxy flavone **(2)**, 5,7-dihydroxy -3,3',4'-trimethoxyflavone **(3)**, Bonanzin **(4)**, 3,5,6,7,4'-pentamethoxy flavone **(5),** a sesquiterpene, Cryptomeridiol **(6)** and stigmast-5,22-dien-3-O-β-D-glucopyranoside **(7)**. The anti-inflammatory activity of compounds **2** and **5** was assessed *in vitro* on CaCo2 cells stimulated by lipopolysaccharide (LPS). Both compounds downregulated LPS-induced expression of inflammatory cytokines; tumor necrosis factor alpha (TNFα), interleukin 1β (IL1β), nuclear factor kappa B (NFκB), cyclooxygenase 1 (Cox1), cyclooxygenase 2 (Cox2), and 5-lipoxygenase (5Lox). In vivo, both compounds significantly decreased paw edema thickness in rats relative to carrageenan, showing better anti-inflammatory activity than celecoxib (36.98%) after 1h (46.60% and 48.11%, respectively). An *in silico* study was performed, where both compounds were docked into the active site of the crystal structure of the human Cox2 enzyme.

Keywords: *Chiliadenus montanus*; methoxyflavonoids; cytokines; colorectal cancer; docking.

Experimental section

Plant materials

Chiliadenus montanus (Vahl) Brullo *(=Jasonia montana* (Vahl) Botsch.) whole plant (Order Asterales, Family Asteraceae, subfamily Asteroideae, tribe Inuleae) was gathered during the flowering phase in March 2015 from the Sinai Peninsula in Egypt. It was authenticated by the Herbarium Department at the Faculty of Science, Botany Department, Suez Canal University, Egypt. A voucher specimen was deposited in the Herbarium of Pharmacognosy Department, Faculty of Pharmacy, Suez Canal University, Ismailia under registration number SAA-18.

Extraction and isolation of secondary metabolites

Methanolic extraction was performed on 10 Kg of *Chiliadenus montanus* air-dried powder as previously described (Badawy et.al, 2019). Briefly, the powder was macerated in 90 % MeOH for 1 day at room temperature, filtered, and evaporated till

getting 450 g dry extract. A weight of 425 g of the extract was fractionated using silica gel vacuum liquid chromatography (VLC) with gradient elution (n-hexane/EtOAc/MeOH0 to give 6 fractions (4 L each). The fractions were evaporated under reduced pressure and the residues were weighed and refrigerated until further processing.

Fraction **3** (F3, 35 g) was sub-fractionated by silica gel column chromatography (n-hexane/ EtOAc/ MeOH gradient) to give 4 sub-fractions (f1- f4). Subfraction F3-f1 was further purified using a silica gel column eluted with n-hexane/ EtOAc gradient to give two yellow spots. Final purification was done using sephadex column LH-20 using 100% methanol as isocratic eluent giving pale yellow powder (compound **1)**, followed by a sephadex column LH-20 using Methanol: Dichloromethane (1:1) and a pale yellow powder was obtained (compound **2)**. Subfraction F3-f3 (2 g) was subjected to chromatographic purification on flash silica gel column eluted with n-hexane/ EtOAc gradient. Final purification was done using sephadex column LH-20 using Methanol: Dichloromethane (1:1) to yield compound **3**. Upon evaporation of subfraction F3-f4, needle-like light yellow crystals were precipitated on the wall of the test tube. Further purification of the precipitate was performed using preparative TLC using Methanol: Chloroform as a mobile phase to yield compound **4**. Isolation of major compounds from fraction (3) was sketched in scheme (1).

Fraction **4** (F4, 150 g) was subjected to silica gel column chromatography (n-hexane/ EtOAc/ MeOH gradient) to yield 3 sub-fractions f1-f3. Subfraction (F4-f1) was slurred with a small amount of silica gel and eluted with n-hexane/ EtOAc gradient. A yellow precipitate was collected. It was purified by applying on Sephadex LH-20 by using Methanol: Dichloromethane (1:1) resulting in the isolation of a yellow amorphous substance referred to as compound **5**. Subfraction (F4-f2) was purified using a silica gel column eluted with n-hexane/ EtOAc gradient. It was further purified using Sephadex LH-20 and 100% methanol as an isocratic eluent. A white substance that didn't appear under UV lamp was obtained, which gave a bluish violet spot after spraying with anisaldehyde/ H_2SO_4 as a spray reagent. It was identified as compound **6**. Subfraction F4-f3 was purified on a silica gel column eluted with (n-hexane/ EtOAc/ MeOH gradient). A precipitate was obtained and purified by preparative TLC using Methanol: Chloroform to give a pure white

substance identified as compound **7**. Isolation of major compounds from fraction (4) was sketched in scheme (2).

Scheme 1. Isolation of the major compounds from fraction (**3**).

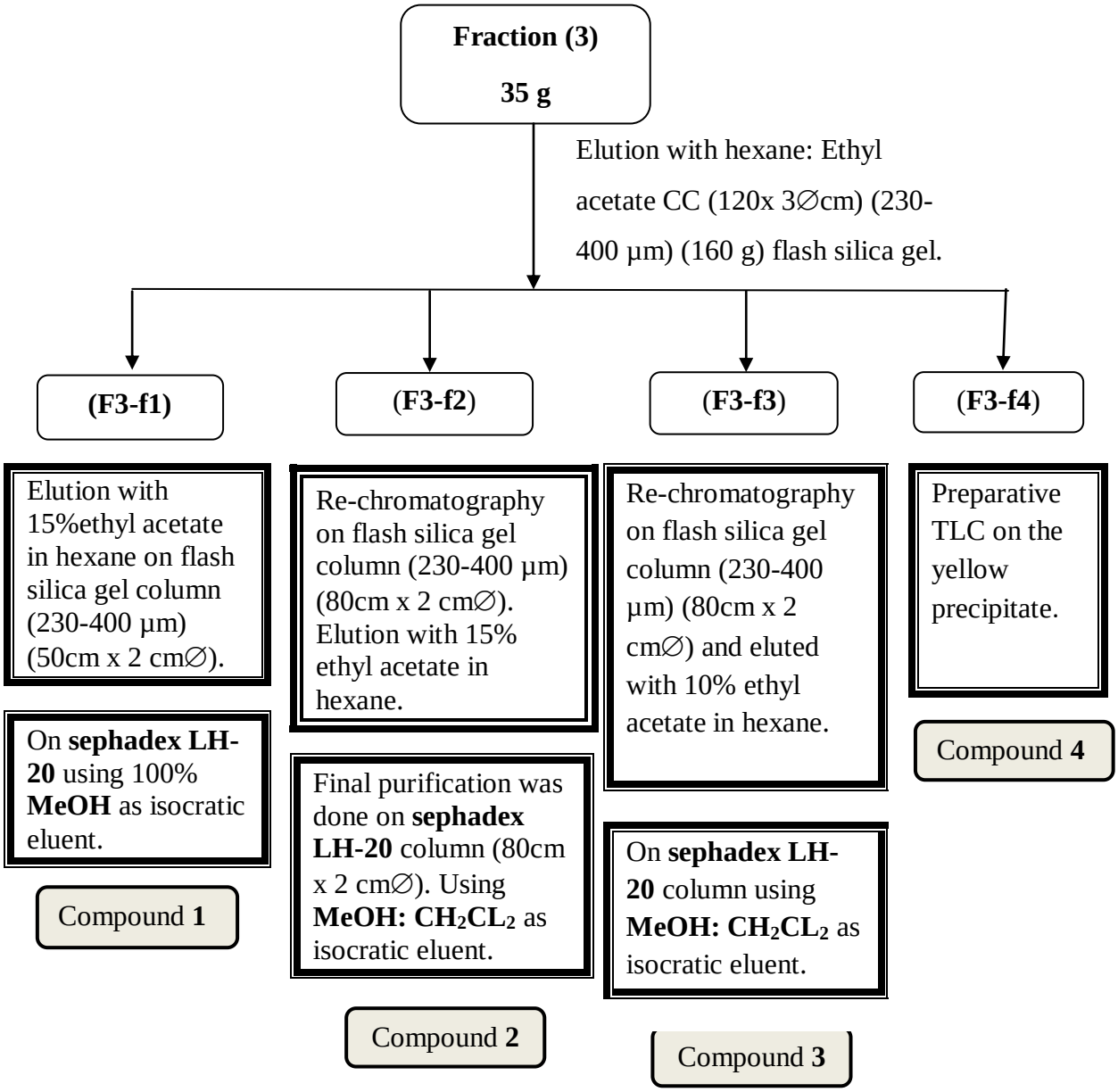

Scheme 2. Isolation of the major compounds from fraction (**4**).

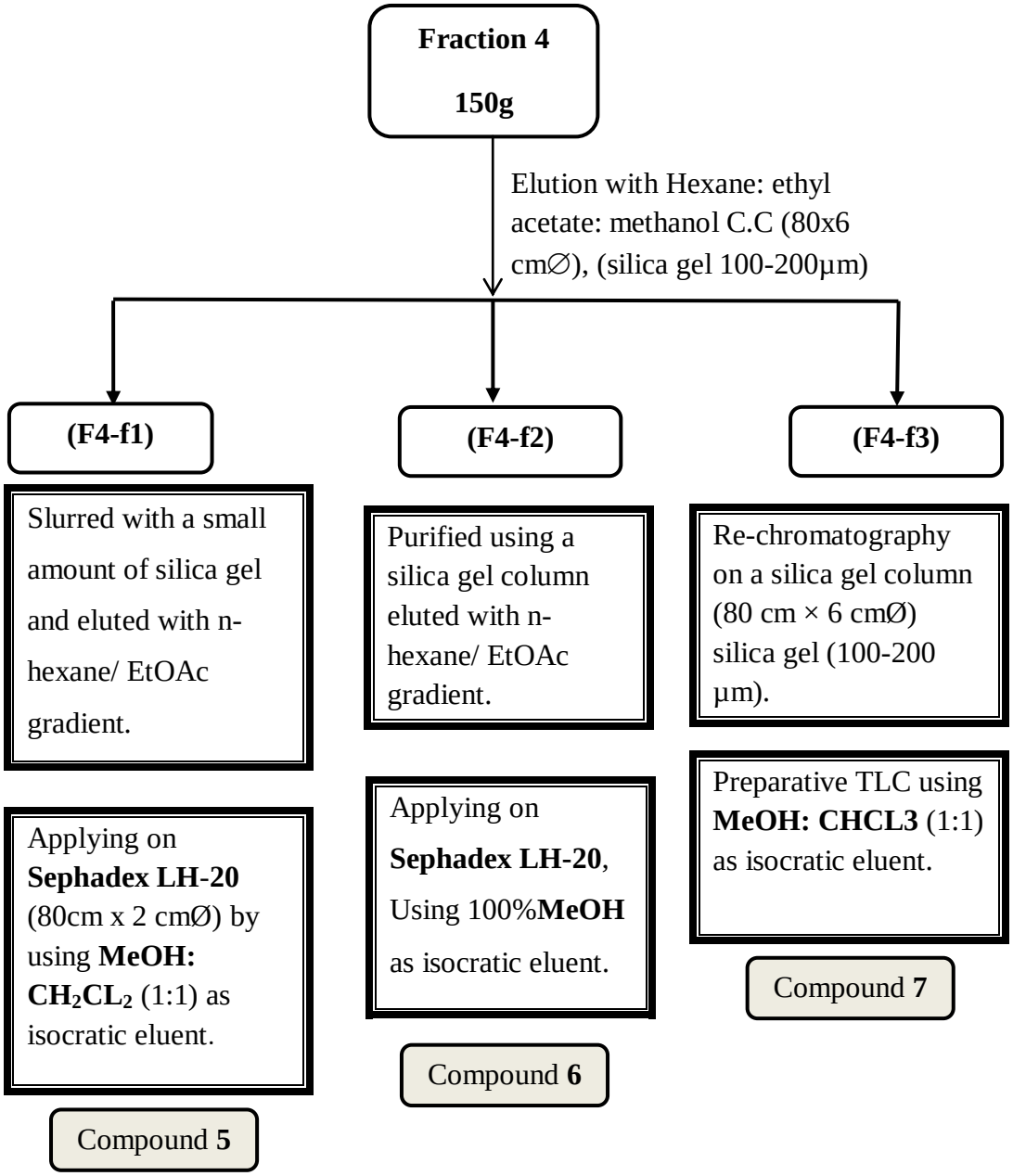

Biological activity of *Chiliadenus montanus*

Cell culture

The adherent colorectal cancer cell line, CaCo2 was obtained from VACSERA, Cairo, Egypt. The cells were cultured in DMEM medium (GIBCO, NY, USA, #11995073) supplemented with 10% heat-inactivated fetal bovine serum (GIBCO, # 10099133), 1% penicillin/streptomycin (Thermo Fisher Scientific, MA, USA, # SV30082) and 2% L-glutamine (Invitrogen, NY, USA, # 25030024) at 37 °C and 5% CO2. Culture renewal was done when the cells reached 80-90% confluence using 0.025% trypsin-EDTA (Invitrogen, # 25200056).

Determination of cell viability by MTT assay

The influence of the compounds on cell viability of CaCo2 cells was determined by MTT assay [3-(4,5-Dimethylthiazol-2-yl)-2,5-diphenyltetrazolium bromide, purchased from Molecular probes, Oregon, USA, # V-13154]. The tested compounds and cisplatin as a standard were added at serial concentrations from 8.35 to 302.76 µM, followed by the addition of 12 mM MTT solution (10 µl/well) and incubation for 4 hours at 37 °C. Colour reaction was initiated by 100 µl DMSO (Sigma Aldrich, USA, # 673439) for 20 minutes and the optical density was measured at an absorbance of 570 nm using an Elisa reader (StatFax-2100, Awareness Technology, Inc., USA). The concentration of the compounds that killed 50 % of cells (inhibition concentration, IC_{50}) was computed using the sigmoidal curve. Assays were carried out in triplicate in three independent experiments.

Experimental groups

The CaCo2 cells were divided into the following three groups (G1-G3); G1 (normal control group) with no treatment, G2 (LPS group) cells treated with 1 µg/ml lipopolysaccharides (LPS) which was previously reported to induce inflammation in CaCo2 cells (Sanchez-Munoz et al., 2008; Triantafilou et al., 2005; Wang et al, 2013; Yang et al., 2019), G3 (compound 2-treated cells) and G4 (compound 5-treated cells) cells treated with 1/10 IC_{50} of compounds **2** and **5**, respectively. In G3 and G4, CaCo2 cells were first treated with 1/10 IC_{50} of compound 2 or 5 for 1 h and then with 1 µ*g*/mL LPS. After incubation for 24 h, the cells were harvested and either stored at -80ºC until RNA extraction or homogenized for measurement of inflammatory cytokines. The 1/10 IC50 dosage was selected because compounds **2** and **5** displayed a lower toxicity at this concentration, which ensures a lower death rate. CaCo2 is the

most well-established cell line for investigating intestinal barrier integrity and function and it was previously used as an *in vitro* model for inflammation induced by LPS to investigate the anti-inflammatory effect of natural compounds (Sanchez-Munoz et al., 2008; Triantafilou et al., 2005; Wang et al, 2013; Yang et al., 2019). For these reasons, CaCo2 was selected to investigate the anti-inflammatory effect of compounds **2** and **5** in the present study.

Detection of inflammatory parameters by Elisa

The levels of inflammatory parameters [tumor necrosis factor-alpha (TNFα), interleukin 1 beta (IL1β), nuclear factor kappa B (NFκB), cyclooxygenase 1 (Cox1), Cox2, and 5-lipoxygenase (5Lox)] were measured as previously described (Karan et al., 2018). In brief, the cells were seeded at 5×10^4 cells/well in 96-well plates. Compounds **2** and **5** (1/10 IC_{50}) and LPS (1 μg/mL) were added to the culture medium and incubated at 37 °C for 24 h. The medium was collected in a microcentrifuge tube and centrifuged at 1500 rpm for 10 min. The supernatant was decanted into new microcentrifuge tubes, and the level of TNFα, IL1β, NFκB, Cox1, Cox2, and 5Lox were determined using commercial Elisa kits (Gayman Chemical, Ann Arbor, MI, USA) with the following cat # MBS2502004, MBS772107, MBS450580, MBS026381, MBS731300, and MBS2600640, respectively.

Real-time PCR

Real-time PCR (qPCR) was applied to assess the effect of the compounds on the relative expression of proinflammatory genes in inflamed CaCo2 cells. First, total RNA was extracted from cells using a commercial kit (Thermo Scientific, USA, #K0731) as previously described (El-Magd et al., 2018). Second, RNA concentration and purity were assessed by a Nanodrop (Quawell, Q3000, USA) and was reverse transcribed into cDNA using a commercial kit (Thermo Scientific, #EP0451). Third, specific primers for *TNFα*, *IL1β*, *NFκB*, *Cox1*, *Cox2*, *5Lox*, and *β-actin* (internal reference) genes were created by Primer 3 (Table S1). Finally, qPCR was carried out in StepOnePlus thermal cycler (Applied Biosystem, USA) using qPCR master mix (QuantiTect SYBR Green, Thermo scientific, USA, cat # K0221) in the presence of primers and cDNA. The temperature and duration of qPCR cycles were performed as previously described (Selim et al., 2019). Relative expression was calculated using the $2^{-\Delta\Delta Ct}$ method.

In vivo anti-inflammatory assay

Compounds **2** and **5** and the reference drug celecoxib were evaluated for their anti-inflammatory activities using the *in vivo* carrageenan-induced rat paw edema model with a dose of 50 mg/kg. Carrageenan (λ-Carrageenan, type IV from Sigma, USA) was prepared by dissolving 0.05 g in 5 ml distilled water. Paw thickness was measured after 1, 3, and 5 h of carrageenan injection (Abdellatif et al., 2019).

Table S1. Primers used in qPCR.

Gene	Forward primer ($^{/}5$ ------ $^{/}3$)	Reverse primer ($^{/}5$ ------ $^{/}3$)
TNFa	CCCAGGGACCTCTCTCTAATC	ATGGGCTACAGGCTTGTCACT
IL1β	ACAGATGAAGTGCTCCTTCCA	GTCGGAGATTCGTAGCTGGAT
Cox2	CCCTTGGGTGTCAAAGGTAA	GCCCTCGCTTATGATCTGTC
Cox1	AAGGAGATGGCAGCAGAGTT	GTGGCCGTCTTGACAATGTT
5Lox	ATTGCCATCCAGCTCAACCAA ACC	TGGCGATACCAAACACCTCAG ACA
β-actin	CGACATCAGGAAGGACCTGTA TGCC	GAAGATTCGTCGTGAAAGTCG

Statistical analysis

Experimental data were expressed as means ± standard error of mean (SEM). The statistical significance was estimated by one-way analysis of variance (ANOVA) using GraphPad Prism 8 (LaJolla, CA, USA) followed by Tukey's Honestly Significant Difference (Tukey's HSD) test. Values were considered statistically significant when $p<0.05$.

Docking study

A docking study was performed to gain insight into the possible binding interactions of compounds **2** and **5** with the human Cox2 crystal structure (PDB ID: 5IKQ) (Orlando and Malkowski, 2016). The recently published crystal structure of human Cox2 in complex with Meclofenamic acid (PDB ID: 5IKQ) was used for molecular docking. Compounds **2** and **5** were docked into the active site of the enzyme using the Dock module within Molecular Operating Environment software (MOE 2014.0901, 2014, Chemical Computing Group, Canada). The active site of Cox2 is divided into three important regions; a hydrophobic pocket defined by Tyr385, Trp387, Phe518, Ala201, Tyr248, and Leu352, the entrance of the active site defined by the

hydrophilic residues Arg120, Glu524, Tyr355, and a side pocket lined by His90 Arg513 and Val523 (Llorensa et al., 2002). Compounds were sketched and minimized in MOE using the MMFF94 force field. The binding site was specified using the ligand, Meclofenamic acid, atoms. Docking was performed using the default settings and the Triangular Matcher method within MOE. Thirty docking poses for each compound were generated. The results were analyzed using Pymol graphical software v2.3.

Identification of isolated compounds

Compound 2 exhibited a dark yellow color in UV light at 356 nm which intensified on exposure to ammonia vapor. The ^{1}H-NMR (DMSO-d6, 400 MHz) spectrum showed peaks at δ_H 6.4 (1H, d, J = 1.6 Hz, H-6), 6.2 (1H, d, J = 1.6 Hz, H-8), 7.6 (1H, d, J =1.3 Hz, H-2′), 6.9 (1H d, J =8.4 Hz, H-5′), 7.54(1H, dd, J =1.6 Hz, 8.4 Hz, H-6′), 12.68 ((1H, br.s., OH at C-5) and two singlet peaks for two methoxy groups protons at δ 3.80–3.86, corresponding to (3, 3′ –OCH3) (Figure S3). The ^{13}C NMR spectrum (DMSO-d6) indicated the presence of 17 signals at δ_C 178.174 (C-4), 56.18 (3′-OCH_3), 60.17 (3-OCH_3), 150.23 (C-4'), 147.92 (C-3'), 138.1 (C-3), 104.6 (C-10) (Figure S4). The UV spectrum of compound 2 in methanol showed absorption (λmax) at 356 nm (Figure S5). The compound proved to have a free 7-hydroxyl group (a peak at 274nm with NaOAC) as well as a free 4'-hydroxyl group (increased intensity of band I by about [+54] nm with NaOMe). The compound was proved to be substituted in position 3' as it showed no shift with $AICl_3$-HCI compared to $AlCl_3$. From the above findings and by comparison with published data (Chiappini et al 1982), compound 2 was identified as 5,7,4' Trihydroxy- 3,3'-Dimethoxy flavone (Figure S11A).

The ^{1}H NMR (DMSO-d6) spectrum of compound 5 showed peaks at δ_H 6.9 (2H, d, J = 8.9 Hz, H-3′/H-5′) 7.9 (2H, d, J = 8.9 Hz, H-2′, H-6′), 7.0 (1H, s, H -8), and five singlet peaks for methoxy group protons at C-5, C-6, C-7, and C-3 while the remaining methoxy group is linked with the ring B at C-4′ as evidenced from the ^{1}H-NMR spectral analysis (Figure S8). The ^{13}C NMR (DMSO-d6) spectrum showed 16 carbon atoms. δ_C 130.2 (C-2', C-6'), δ_C 115.9 (C-3', C-5'), δ_C 97.2 (C-8), δ_C 140.0 (C-3), δ_C 151.7 (C-5), δ_C 139.9 (C-6), δ_C 157.8 (C-7) (Figure S9). From the above findings in addition to the MS spectrum (Figure S10) and by comparison with

published data (Horie et al., 1998), compound 5 was identified as 3,5,6,7,4'-pentamethoxy flavone (Figure S11B).

The ^{1}H NMR and ^{13}C NMR spectra of compounds **1, 2, 4,** and **5** were presented in figures S1- S9. The ^{1}H NMR and ^{13}C NMR signals of compounds **1, 2, 4,** and **5** were presented in Tables S2-S5. Compounds **3**, **6**, and **7** were not tested due to lack of availability.

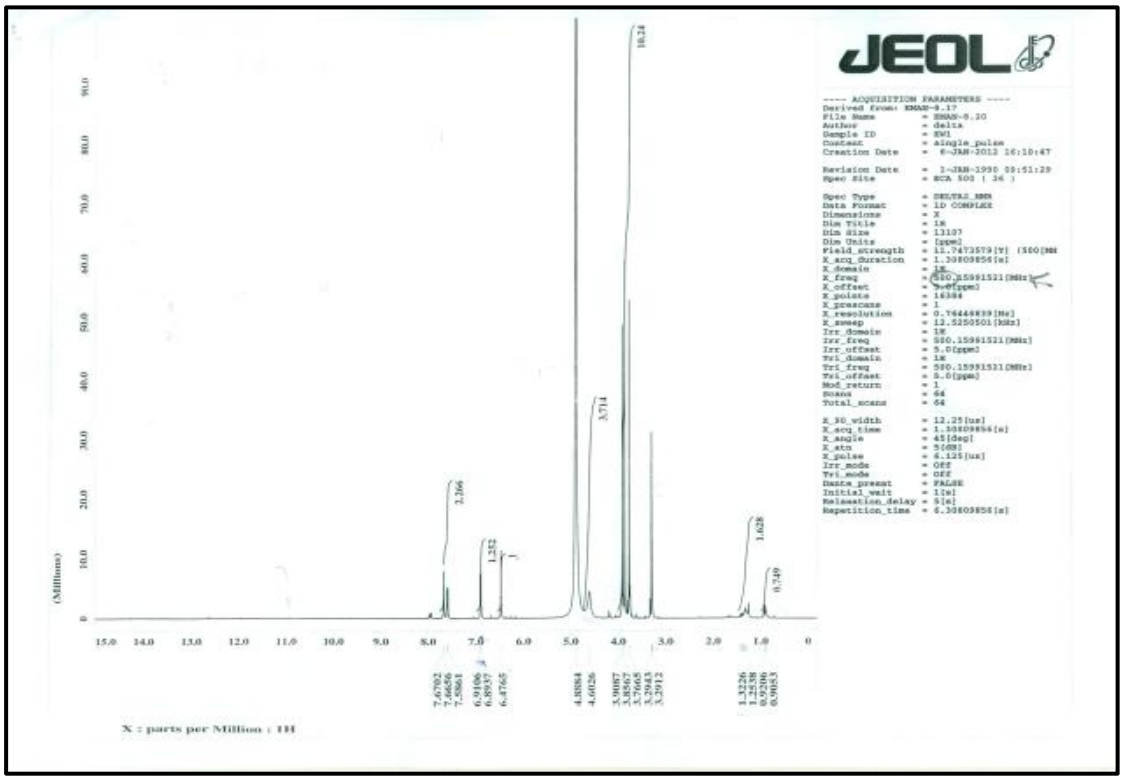

Fig. S1. ^{1}H NMR spectrum of compound **1**.

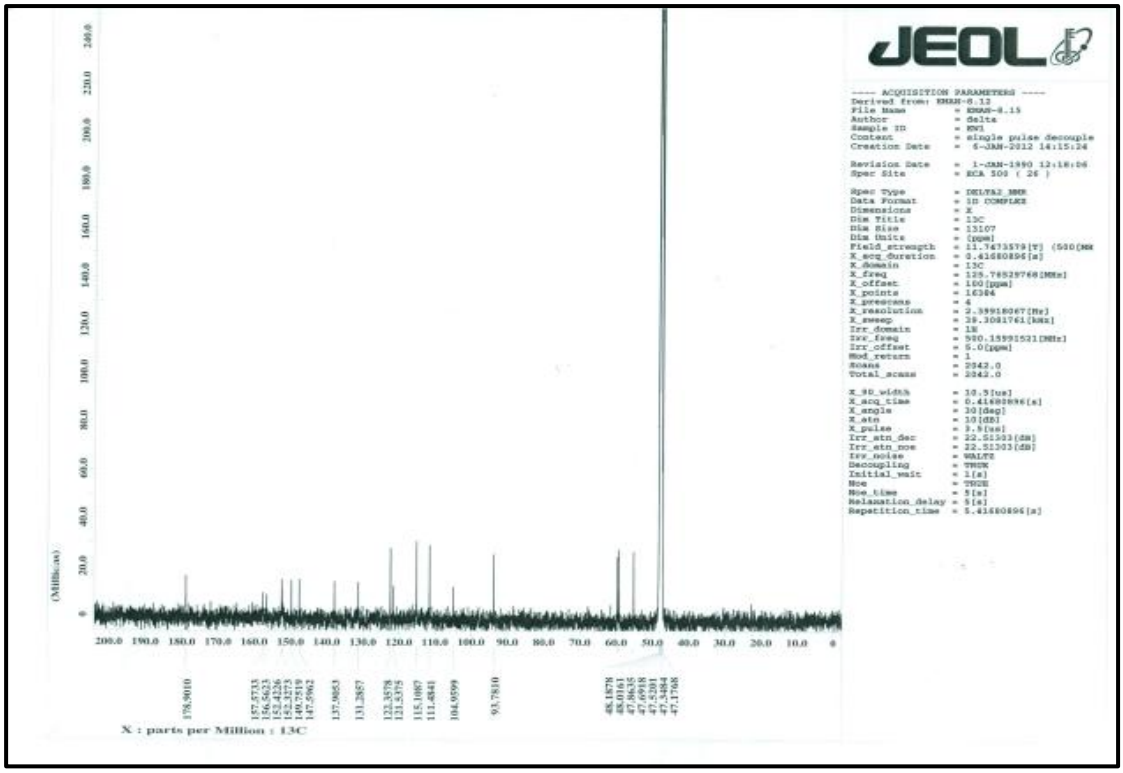

Figure S2. ^{13}C NMR spectrum of compound **1**.

Table S2. ^{1}H (400 MHz) and ^{13}C (100 MHz) NMR spectroscopic data of compound 1.

Carbon No.	^{13}C (δ,PPM)	^{1}H (δ,PPM)
2	152.3	
3	137.9	
4	178.9	
5	152.5	
6	131.2	
7	157.5	
8	93.7	6.5(1H,S)
9	156.5	
10	104.9	
1'	122.3	
2'	115.1	7.6(1H,d, J=2.0)
3'	147.5	
4'	149.7	
5'	111.4	6.9(1H,d, J=8.4)
6'	121.5	7.5(1H,dd, J=8.2,2.0)

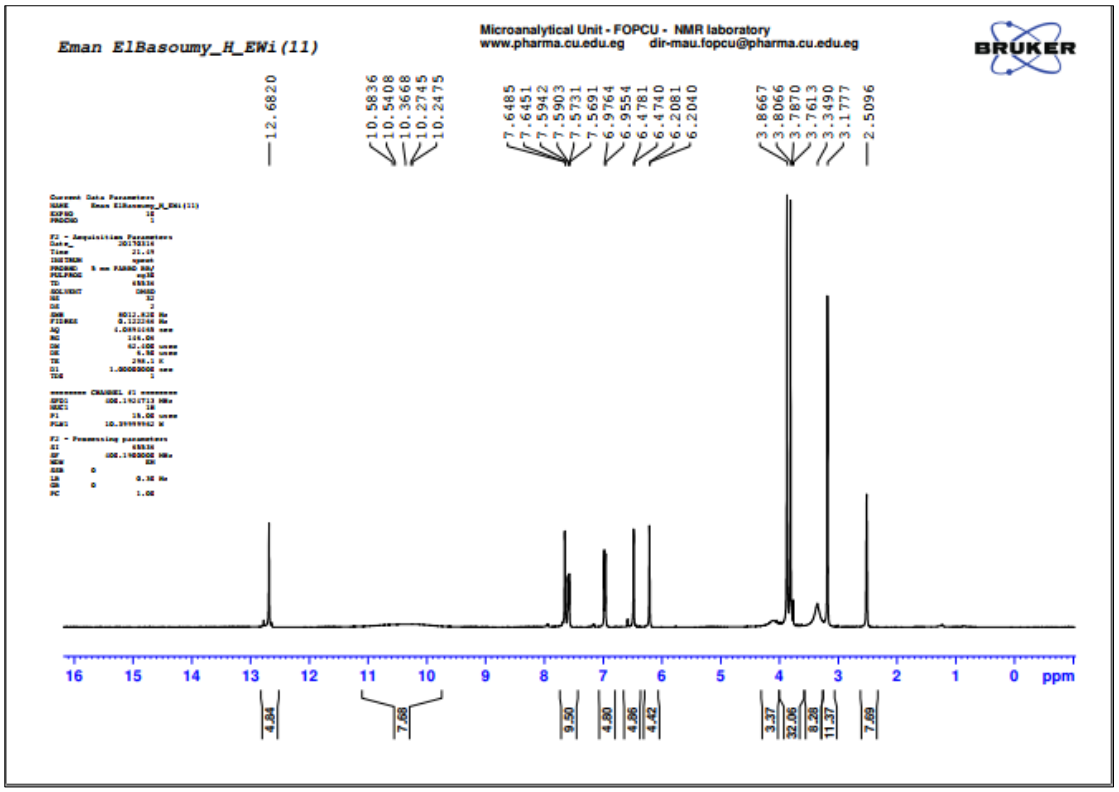

Figure S3. [1] H NMR spectrum of compound **2**.

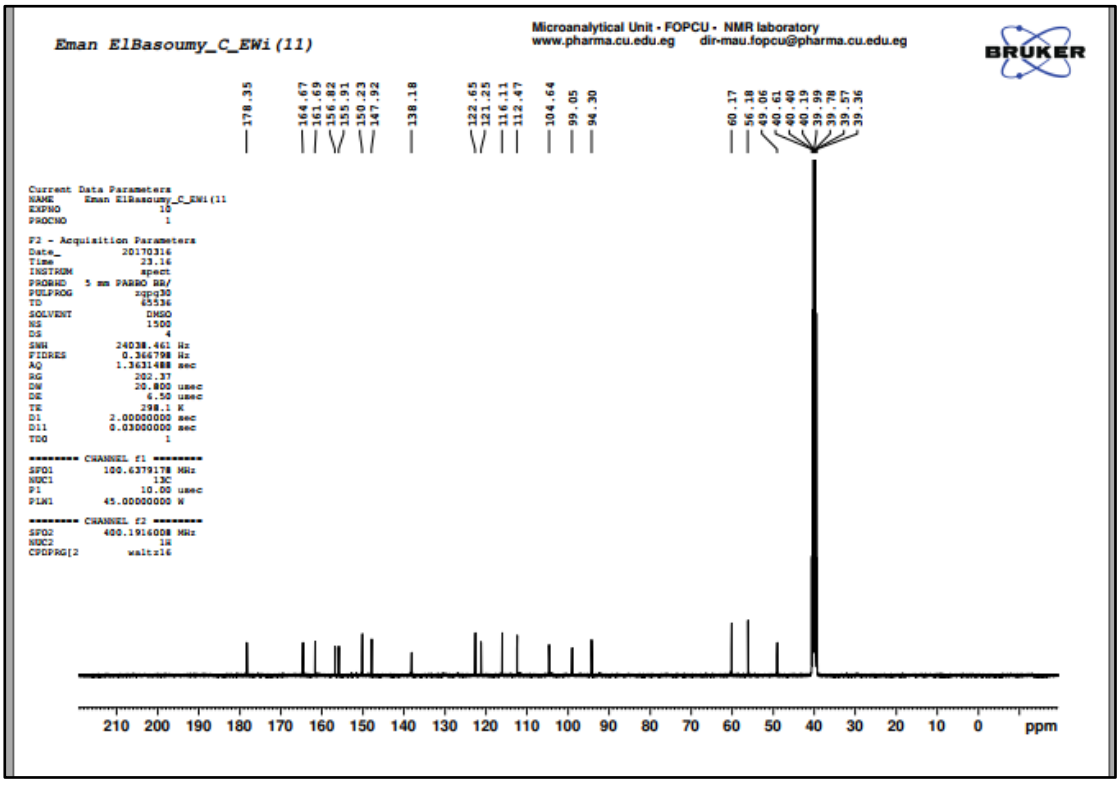

Figure S4. [13] C NMR spectrum of compound **2**.

Table S3. ^{1}H (400 MHz) and ^{13}C (100 MHz) NMR spectroscopic data of compound **2**.

Carbon No.	^{13}C (δ,PPM)	^{1}H (δ,PPM)
2	155.91	
3	138.18	
4	178.35	
5	161.69	12.68(1H,S)
6	99.05	6.2(1H,d,J=1.6)
7	164.67	
8	94.30	6.4(1H,d,J=1.6)
9	156.82	
10	104.64	
1'	121.25	
2'	112.47	7.6(1H,d,J=1.3)
3'	147.92	
4'	150.23	
5'	116.11	6.9(1H,d,J=8.4)
6'	122.65	7.5(1H,dd,J=1.6,8.4)

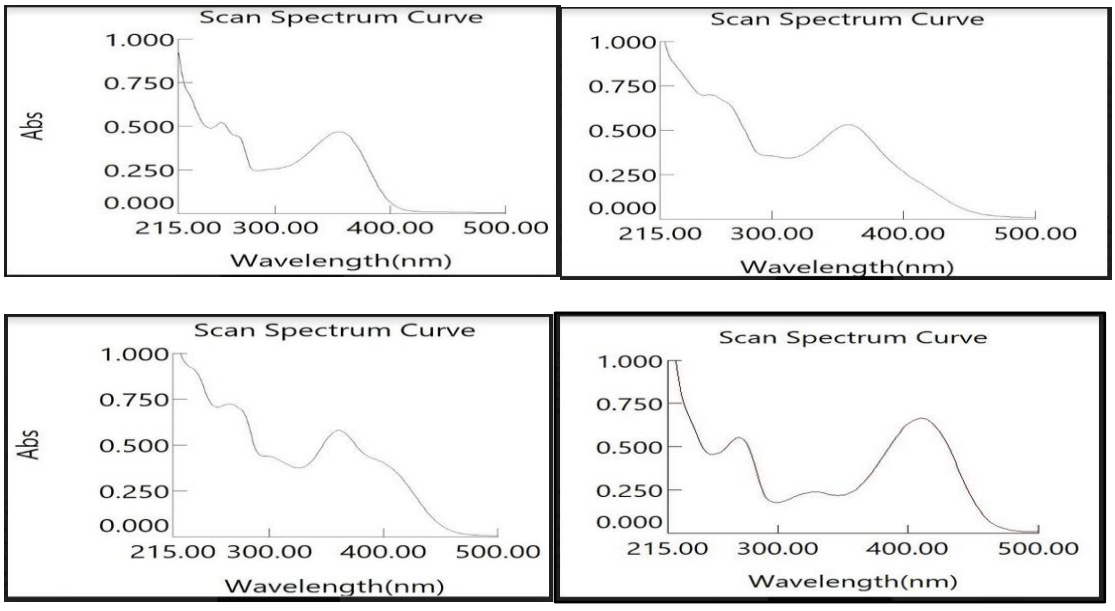

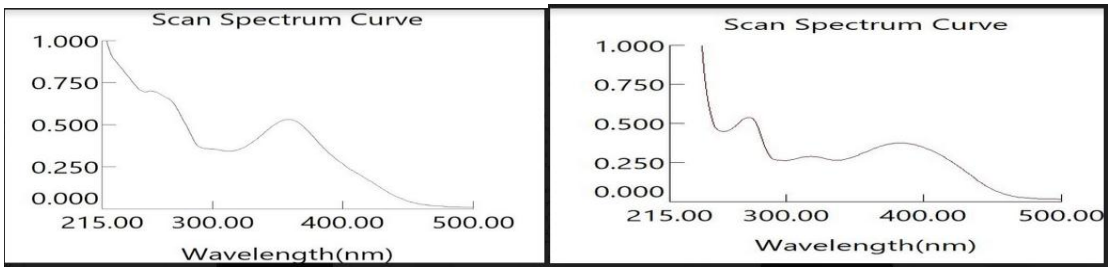

Figure S5. UV spectrum of compound **2**.

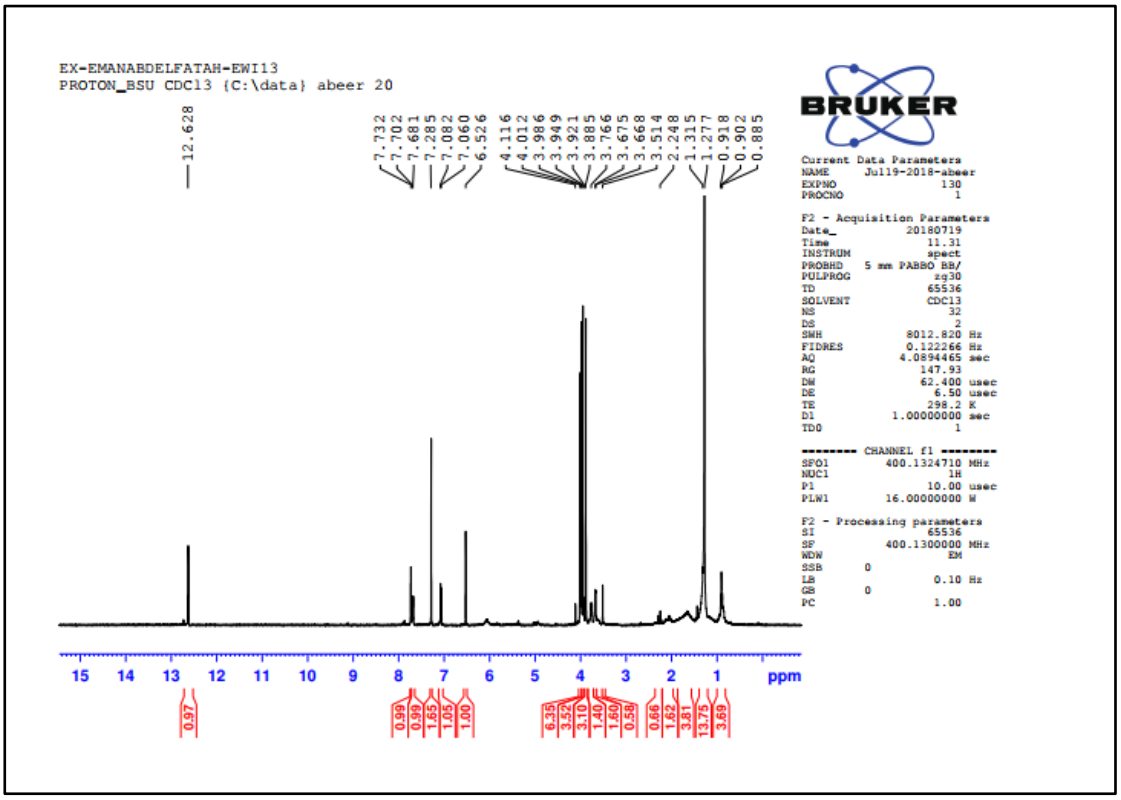

Fig. S6. [1] H NMR spectrum of compound 4.

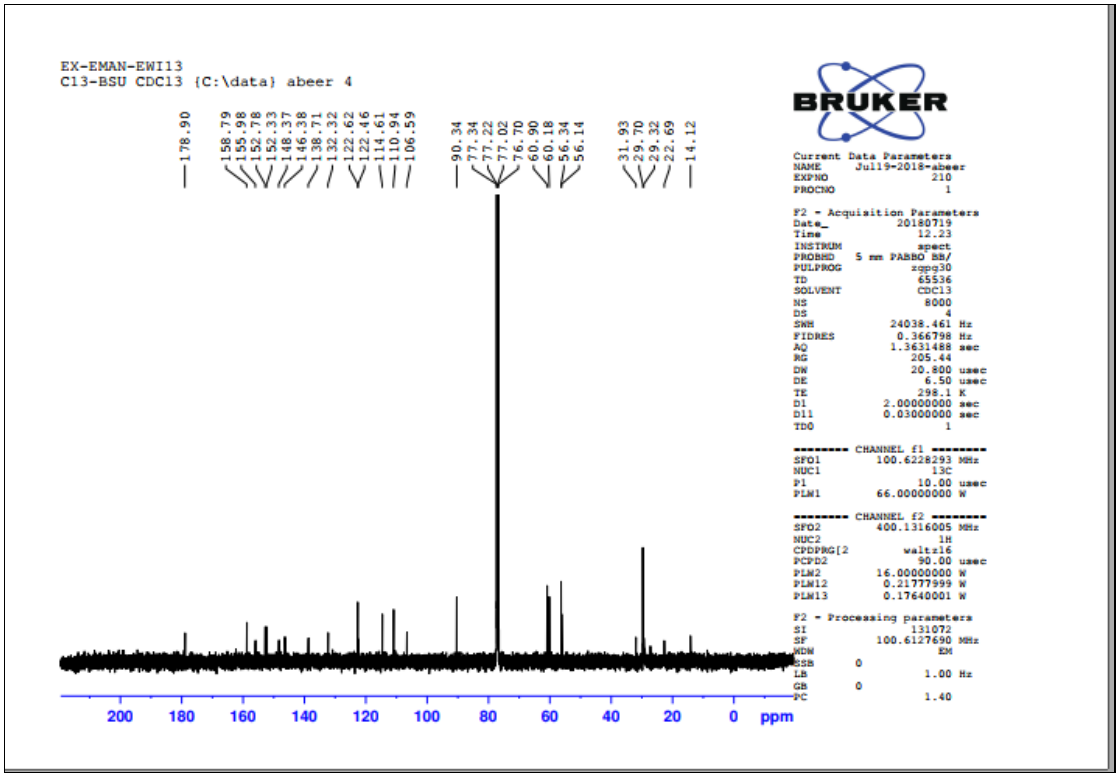

Figure S7. ^{13} C NMR spectrum of compound **4**.

Table S4. ^{1}H (400 MHz) and ^{13}C (100 MHz) NMR spectroscopic data of compound **4**.

Carbon No.	^{13} C (δ,PPM)	^{1}H (δ,PPM)
2	152.78	
3	138.71	
4	178.90	
5	152.33	12.68(1H,S)
6	132.32	
7	158.79	
8	90.34	6.5(1H,S)
9	155.98	
10	106.59	
1'	122.62	
2'	114.61	7.6(1H,d,J=2.4)
3'	146.38	
4'	148.37	
5'	110.94	7.00(1H,d,J=8.8)
6'	122.46	7.7(1H,dd,J=2.4,8.8)

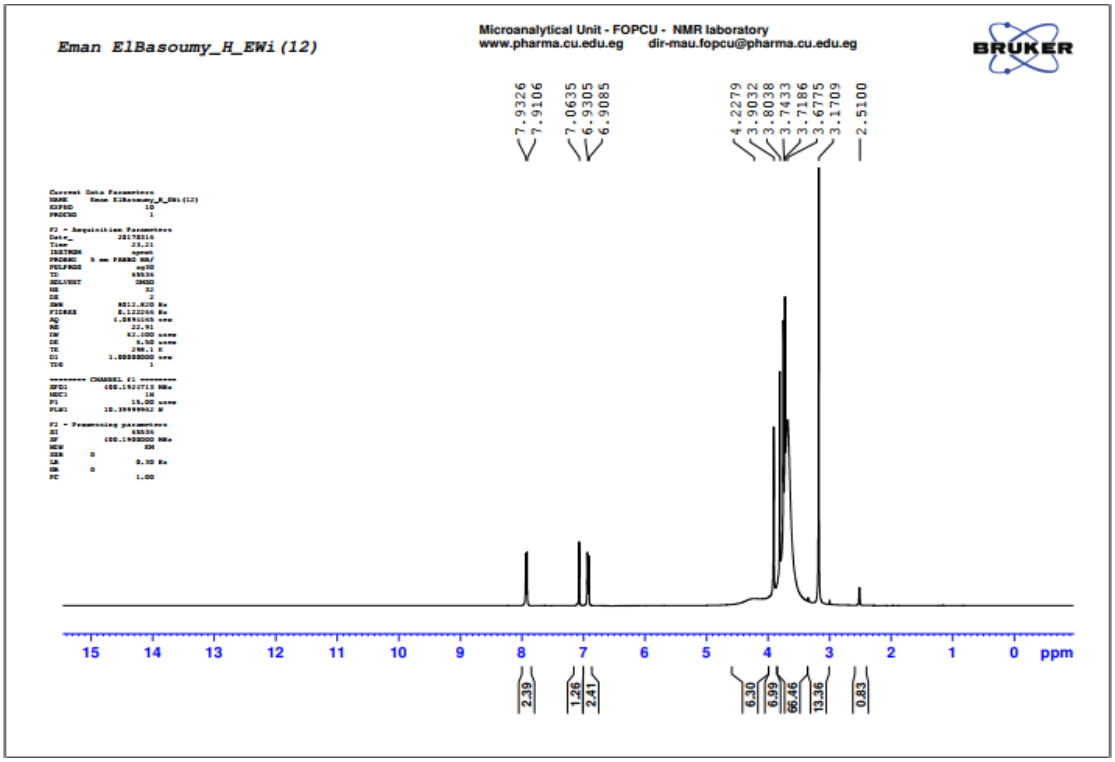

Figure S8. ^{1}H NMR spectrum of compound **5**.

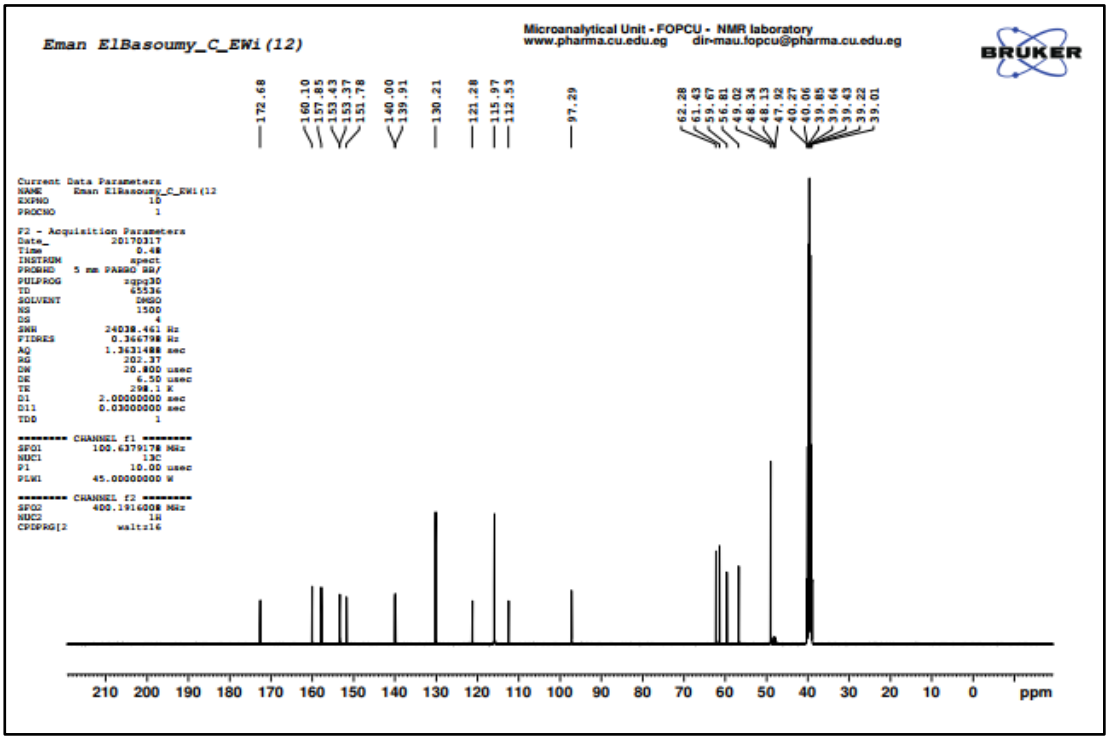

Figure S9. ^{13}C NMR spectrum of compound **5**.

Table S5. ^{1}H (400 MHz) and ^{13}C (100 MHz) NMR spectroscopic data of compound **5**.

Carbon No.	^{13}C (δ,PPM)	^{1}H (δ,PPM)
2	153.3	
3	140.0	
4	172.6	
5	151.7	
6	139.9	
7	157.8	
8	97.29	7.0(1H,S)
9	153.4	
10	112.5	
1'	121.2	
2'	130.2	7.9(2H,d,J=8.9)
3'	115.9	6.9(2H,d,J=8.9)
4'	160.1	
5'	115.9	6.9(2H,d,J=8.9)
6'	130.2	7.9(2H,d,J=8.9)

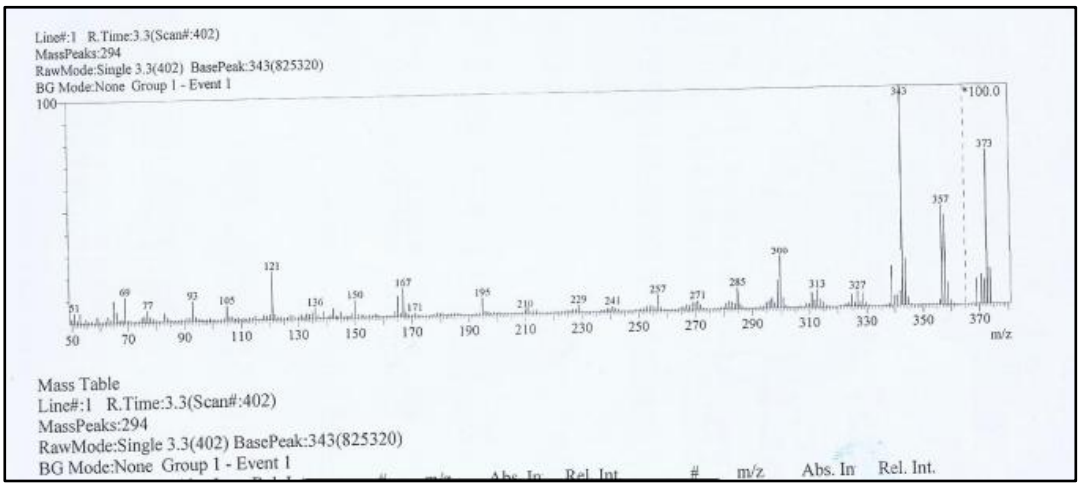

Figure S10. MS spectrum of compound **5**.

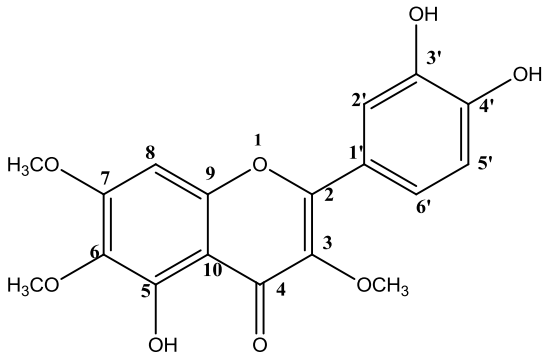

Compound 1

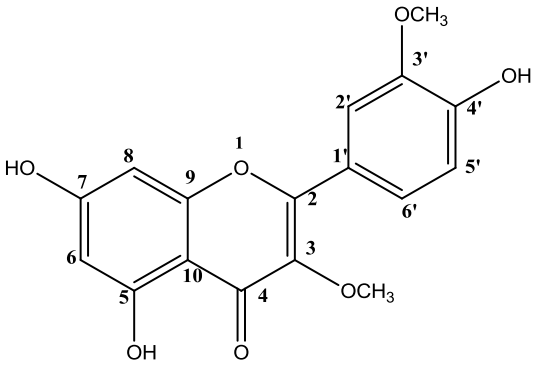

Compound 2

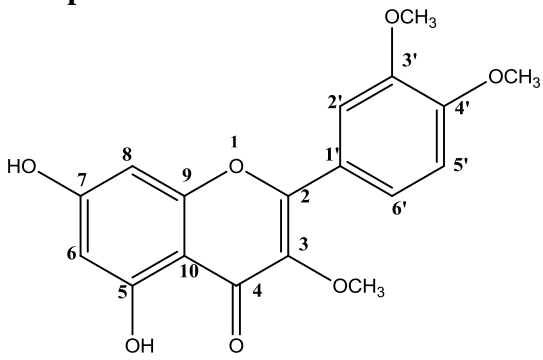

Compound 3

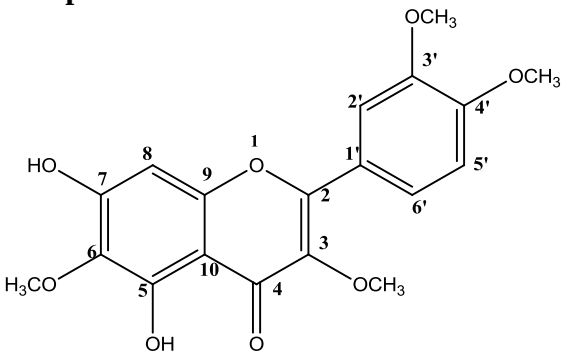

Compound 4

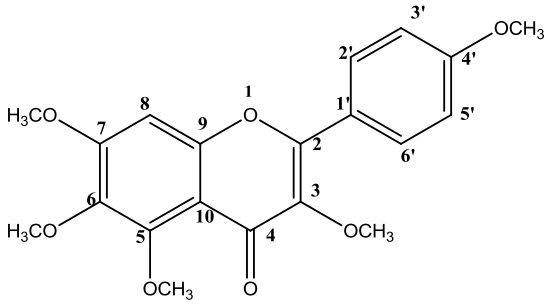

Compound 5

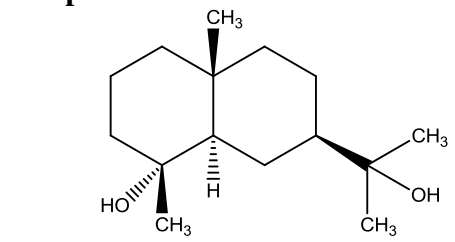

Compound 6

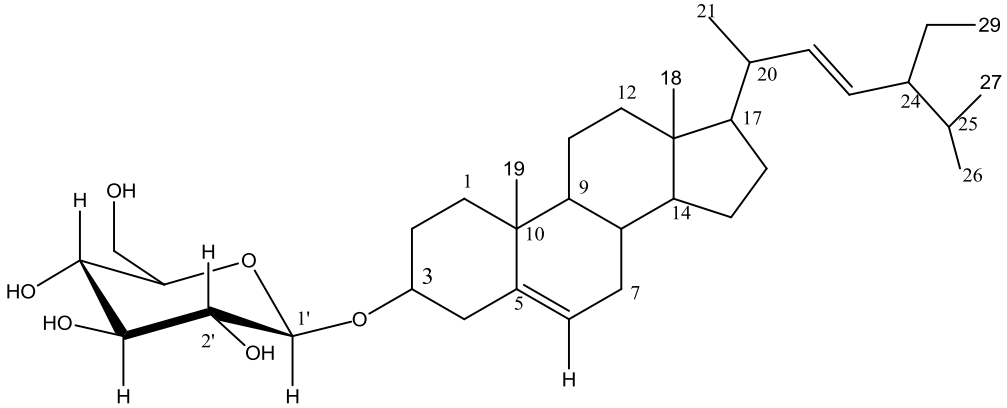

Compound 7

Figure S11. Structures of compounds **1, 2, 3, 4, 5, 6,** and **7**.

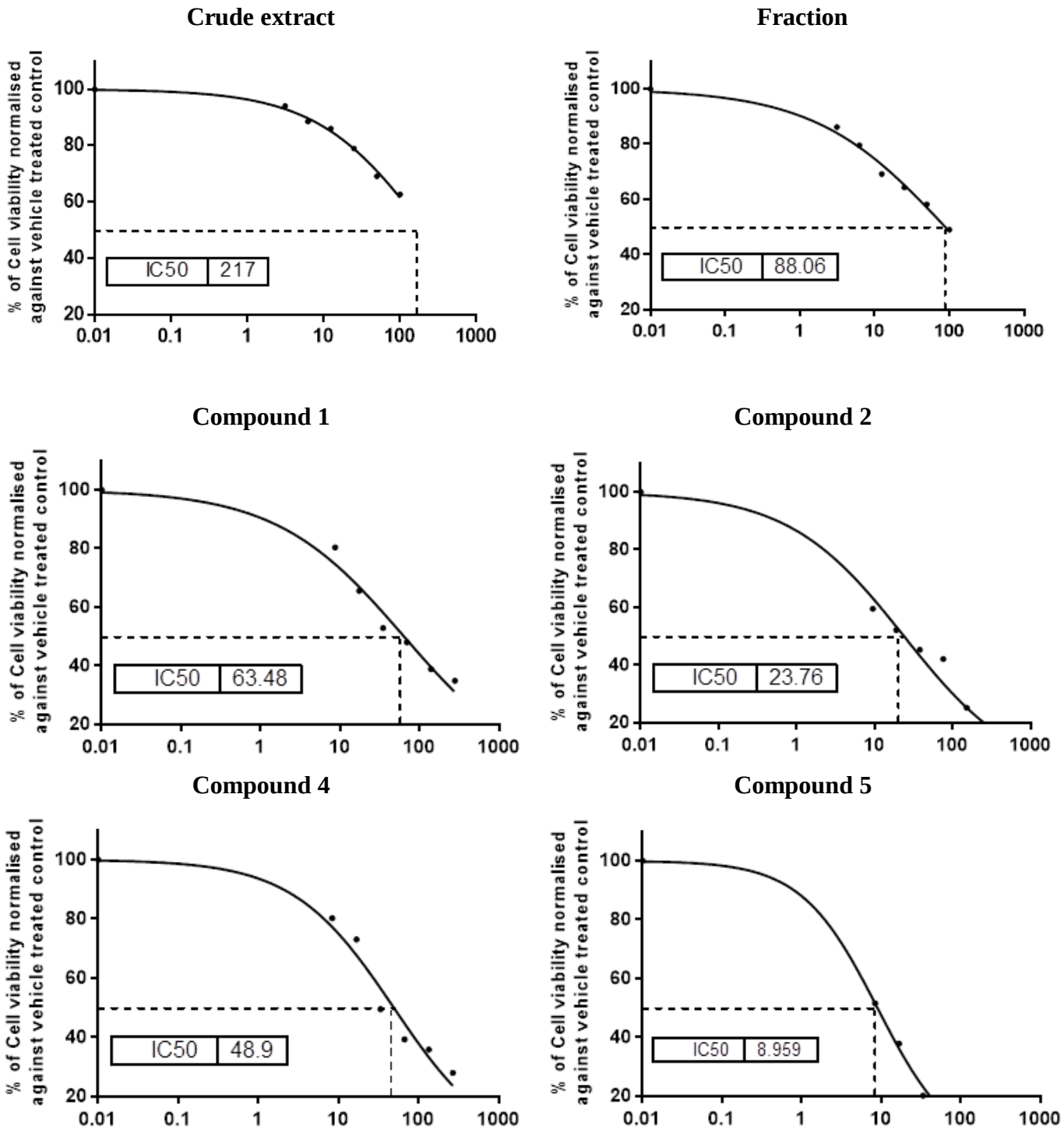

Figure S12. Cytotoxic effect of *Chiliadenus montanus* crude extract, fraction and isolated compounds (**1**, **2**, **4**, and **5**) on CaCo2 cells. Cells were treated with these four compounds at various concentrations ranged from 8.35 to 302.76 µM for 24 hr and the cell viability was determined by MTT assay. The results are expressed as percentage of cell viability relative to vehicle (DMSO)-treated control cells.

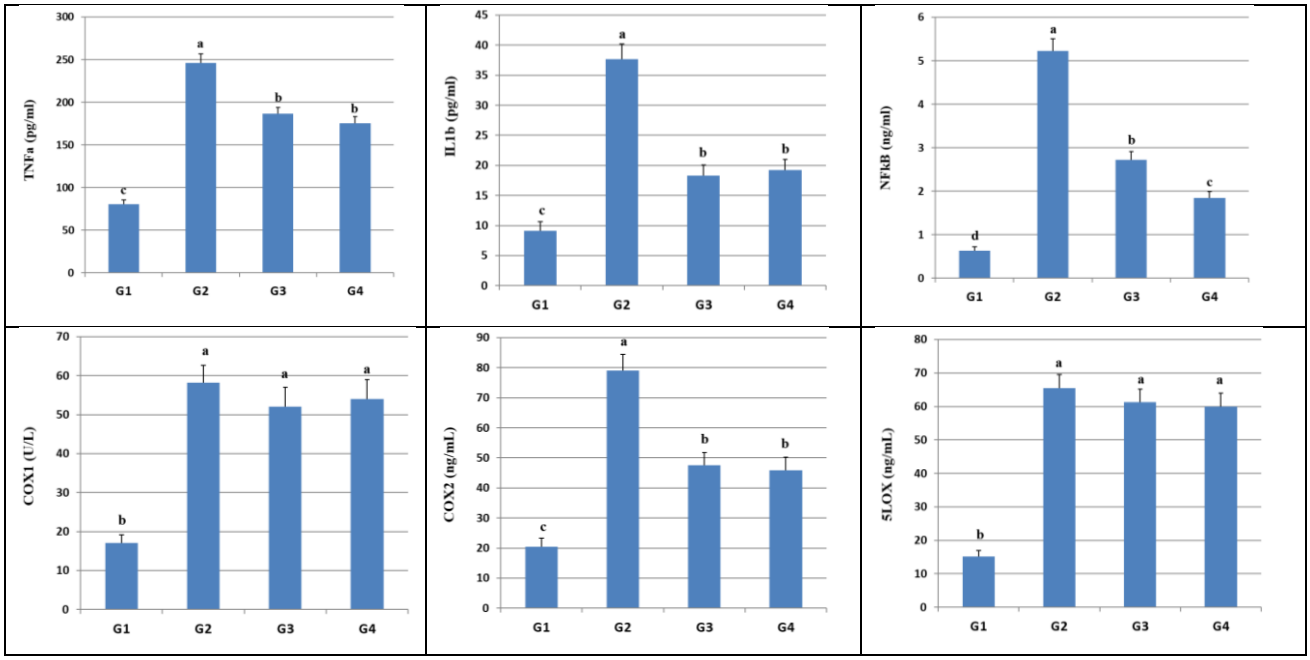

Figure.S13. Effect of compounds **2** and **5** on TNFα, IL1β, NFκB, Cox1, Cox2, and 5Lox levels in LPS-inflamed CaCo2 cells. Data were presented as mean ± SEM (n = 7/group). Means within columns carrying different superscript letters [a (highest values) – c (lowest values)] are significantly different (P≤ 0.05). G1 (control, vehicle treated cells); G2 (untreated LPS-inflamed cells); G3 (compound **2** treated LPS-inflamed cells), and G4 (compound **5** treated LPS-inflamed cells).

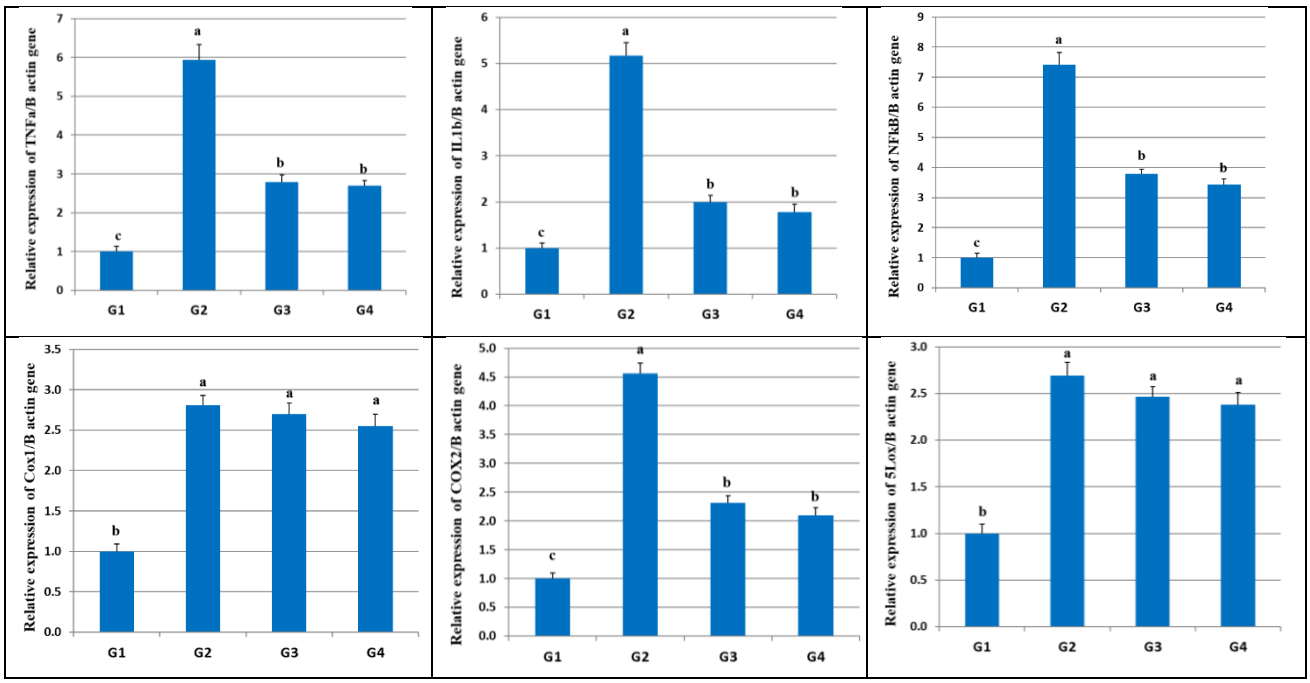

Figure.S14. Effect of compounds **2** and **5** on the relative expression of *TNFα, IL1β, NFκB, Cox1, Cox2,* and *5Lox* genes in LPS-inflamed CaCo2 cells. Data were presented as mean ± SEM (n = 7/group). Means within columns carrying different superscript letters are significantly different (P≤ 0.05).

Table S6. Raw data for qPCR results of the *TNFa* gene.

Group	*TNFa* average cycle threshold (Ct)	Delta Ct	Delta delta Ct	Relative quantification (mean ± SEM)
Control untreated cells (G1)	28.7	0.82	0.00	1.00±0.14
LPS-treated cells (G2)	21.27	-1.75	-2.57	5.94±0.39
Compound 2-treated cells (G3)	27.51	-0.66	-1.48	2.79±0.18
Compound 5-treated cells (G4)	28.36	-0.61	-1.43	2.69±0.14

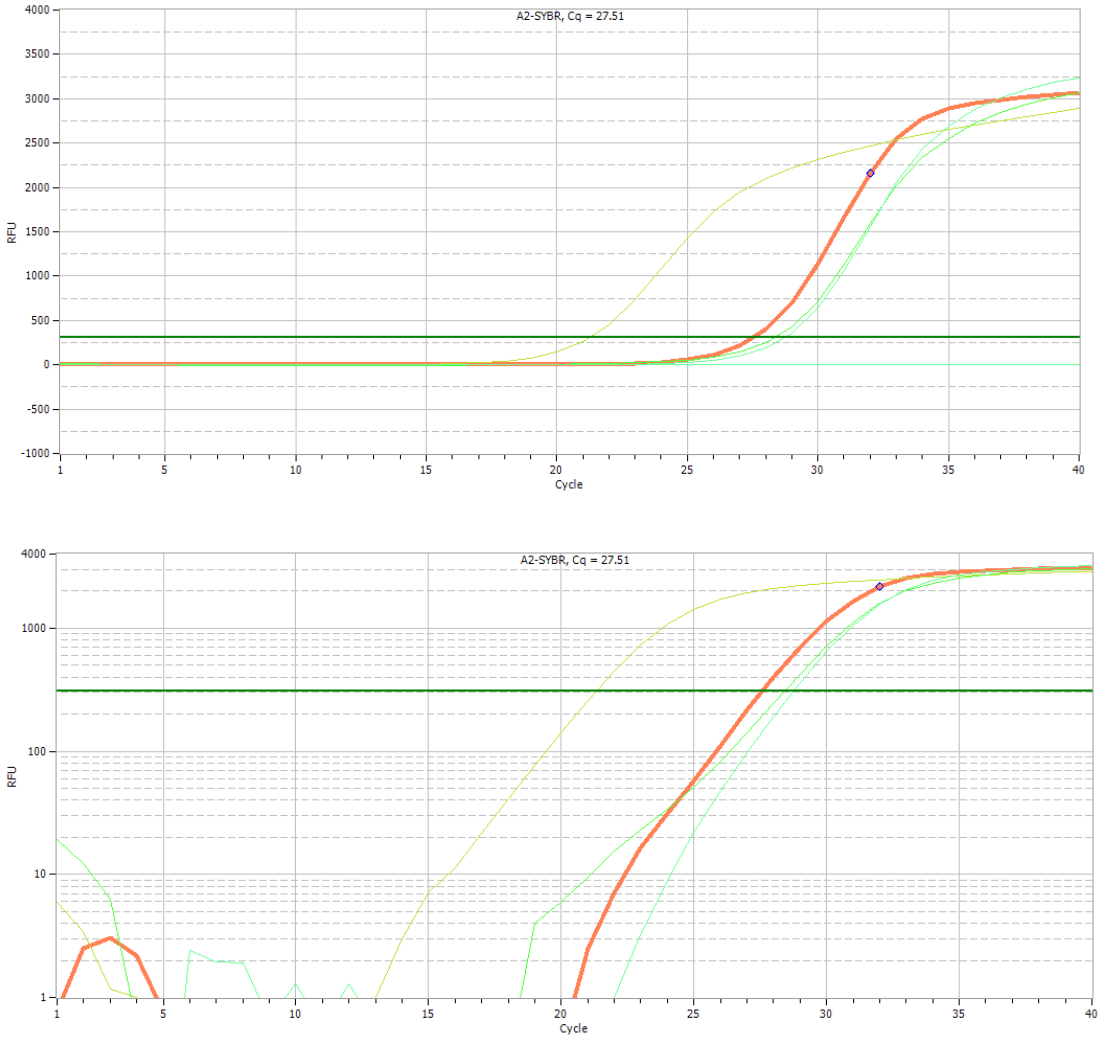

Figure S15. Representative linear (upper) and log (lower) amplification curves representing the Ct values of the *TNFa* gene.

Table S7. Raw data for qPCR results of the *IL1β* gene.

Group	*IL1β* average cycle threshold (Ct)	Delta Ct	Delta delta Ct	Relative quantification (mean ± SEM)
Control untreated cells (G1)	27.03	-0.85	0.00	1.00±0.11
LPS-treated cells (G2)	22.2	-3.22	-2.37	5.17±0.28
Compound 2-treated cells (G3)	25.38	-1.85	-1.00	2.00±0.14
Compound 5-treated cells (G4)	26.32	-1.68	-0.83	1.78±0.17

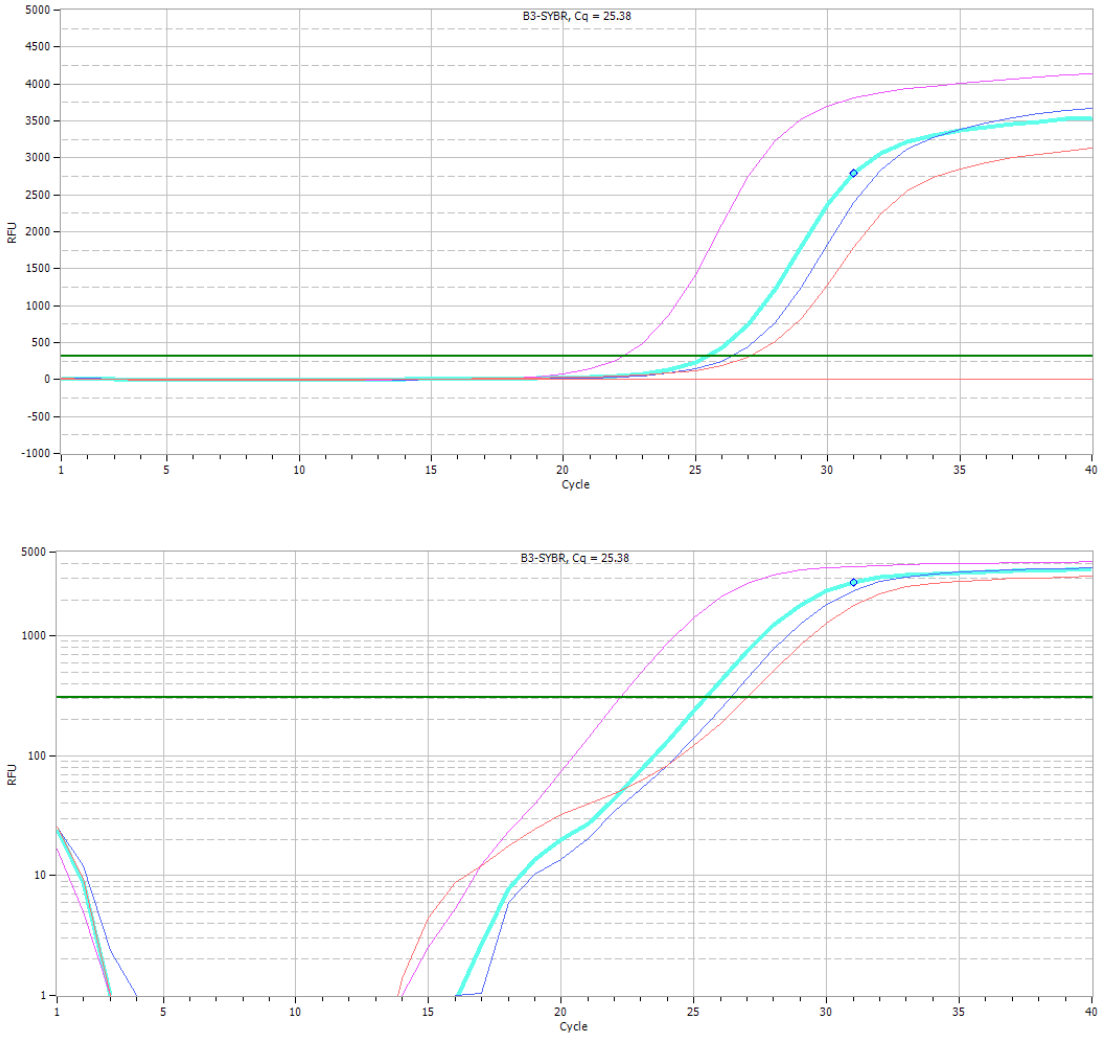

Figure S16. Representative linear (upper) and log (lower) amplification curves representing the Ct values of *IL1β* gene.

Table S8. Raw data for qPCR results of the *NFκB* gene.

Group	*NFκB* average cycle threshold (Ct)	Delta Ct	Delta delta Ct	Relative quantification (mean ± SEM)
Control untreated cells (G1)	29.82	1.94	0.00	1.00±0.15
LPS-treated cells (G2)	25.37	-0.95	-2.89	7.41±0.40
Compound 2-treated cells (G3)	26.55	0.02	-1.92	3.78±0.16
Compound 5-treated cells (G4)	26.57	0.16	-1.78	3.43±0.19

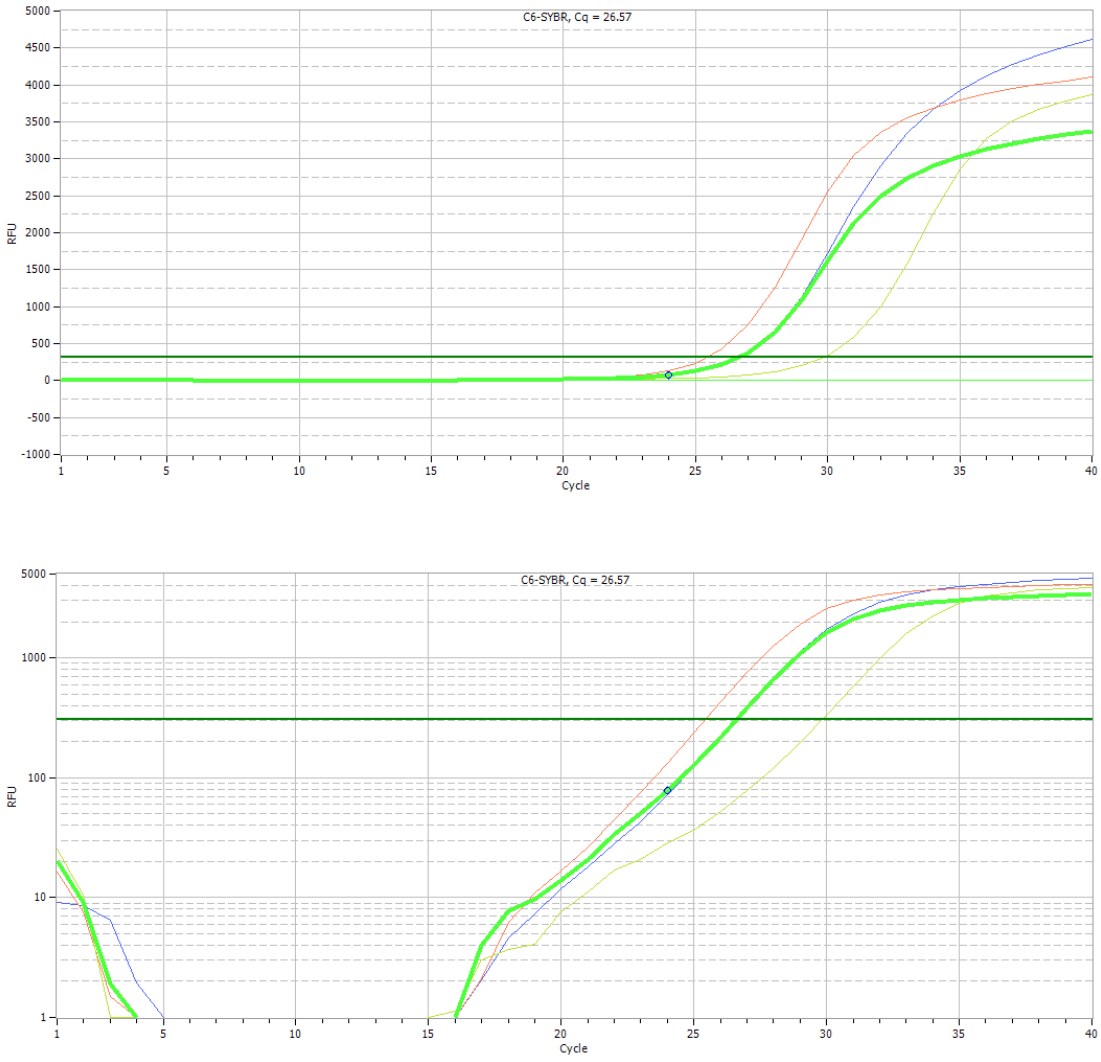

Figure S17. Representative linear (upper) and log (lower) amplification curves representing the Ct values of the *NFkB* gene.

Table S9. Raw data for qPCR results of the *Cox1* gene.

Group	*Cox1* average cycle threshold (Ct)	Delta Ct	Delta delta Ct	Relative quantification (mean ± SEM)
Control untreated cells (G1)	34.53	6.65	0.00	1.00±0.09
LPS-treated cells (G2)	33.48	5.16	-1.49	2.81±0.12
Compound 2-treated cells (G3)	33.65	5.22	-1.43	2.69±0.14
Compound 5-treated cells (G4)	33.71	5.30	-1.35	2.55±0.15

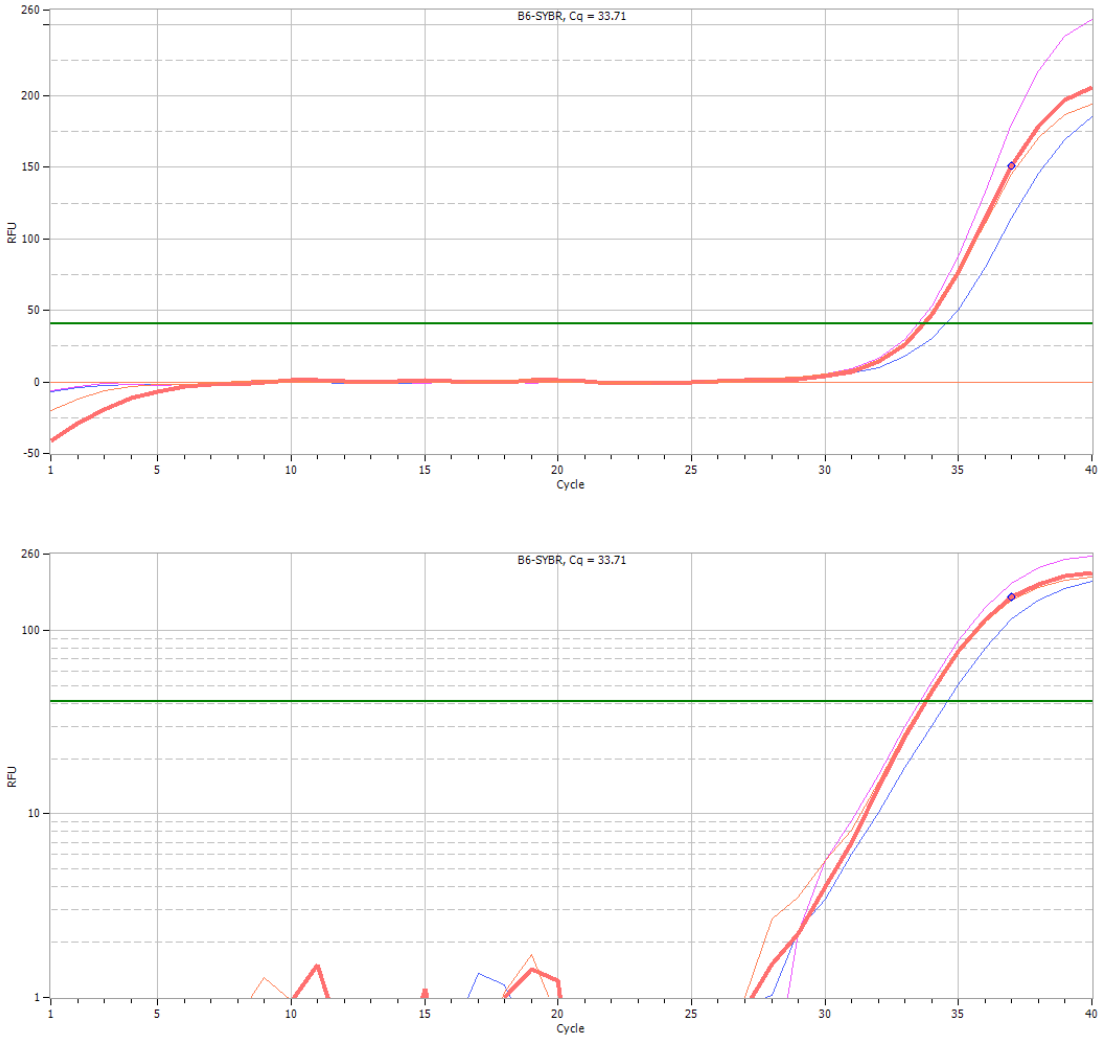

Figure S18. Representative linear (upper) and log (lower) amplification curves representing the Ct values of the *Cox1* gene.

Table S10. Raw data for qPCR results of the *5Lox* gene.

Group	*5Lox* average cycle threshold (Ct)	Delta Ct	Delta delta Ct	Relative quantification (mean ± SEM)
Control untreated cells (G1)	29.17	1.29	0.00	1.00±0.1
LPS-treated cells (G2)	28.18	-0.14	-1.43	2.69±0.14
Compound 2-treated cells (G3)	28.42	-0.01	-1.30	2.46±0.11
Compound 5-treated cells (G4)	28.75	0.04	-1.25	2.38±0.13

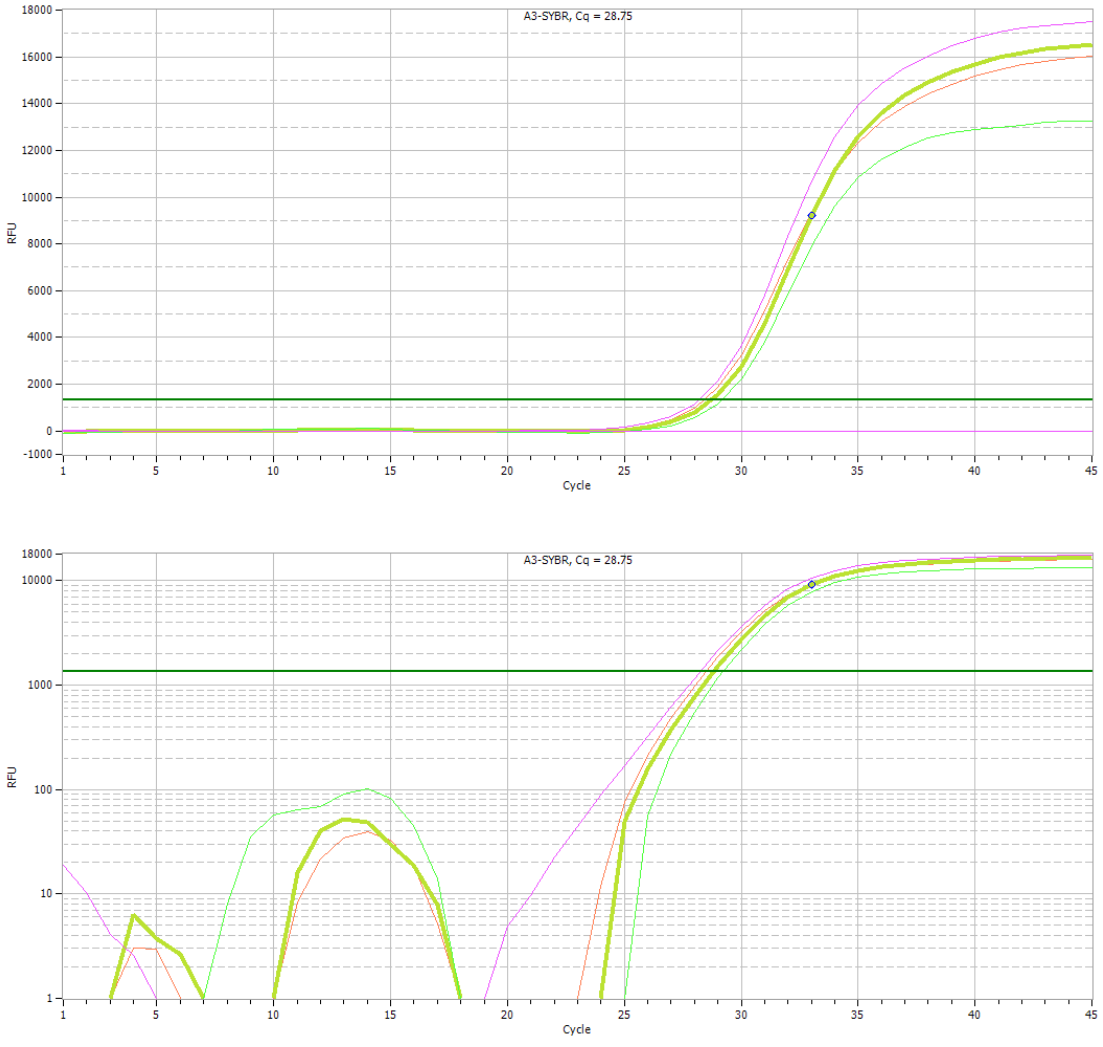

Figure S19. Representative linear (upper) and log (lower) amplification curves representing the Ct values of the *5Lox* gene.

Table S11. Raw data for qPCR results of the *Cox2* gene

Group	*Cox2* average cycle threshold (Ct)	Delta Ct	Delta delta Ct	Relative quantification (mean ± SEM)
Control untreated cells (G1)	27.22	-0.66	0.00	1.00±0.10
LPS-treated cells (G2)	24.77	-2.85	-2.19	4.56±0.18
Compound 2-treated cells (G3)	26.26	-1.87	-1.21	2.31±0.12
Compound 5-treated cells (G4)	26.78	-1.73	-1.07	2.10±0.13

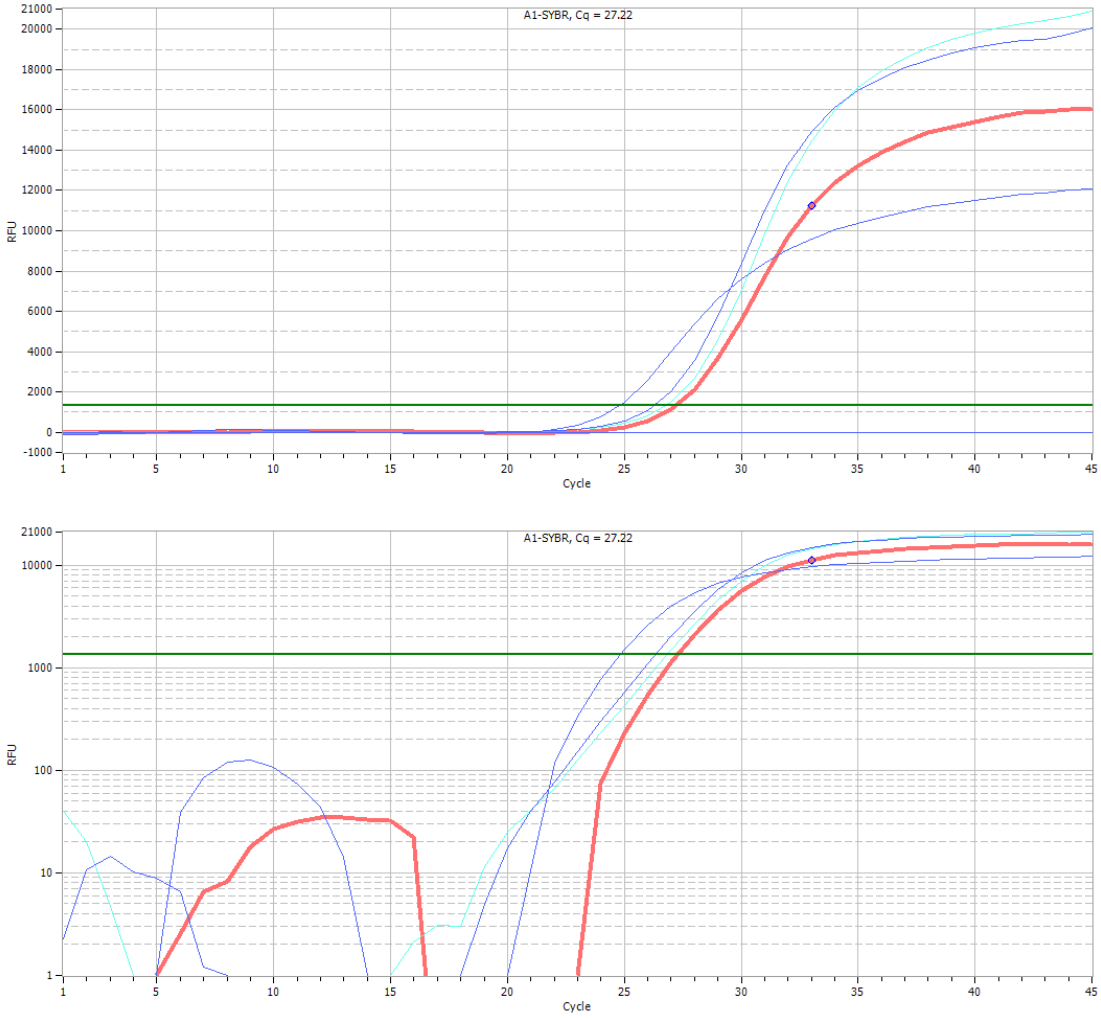

Figure S20. Representative linear (upper) and log (lower) amplification curves representing the Ct values the of the *Cox 2* gene.

Table S12. In vivo anti-inflammatory activity of compounds **2** and **5** and the reference drug celecoxib.

	Mean value of paw edema thickness (cm) ± SEM (% of inhibition)		
	1 h	3 h	5 h
Control (carrageenan)	5.30±0.26 [a]	6.45±0.38 [a]	7.58±0.41 [a]
Compound 2	2.83±0.12 [c] (46.60%)	2.15±0.09 [b] (66.67%)	1.30±0.08 [b] (82.85%)
Compound 5	2.75±0.11 [c] (48.11%)	2.20±0.10 [b] (65.89%)	1.26±0.07 [b] (83.38%)
Celecoxib	3.34±0.12 [b] (36.98%)	1.32±0.10 [c] (79.53%)	0.74±0.06 [c] (90.23%)

Values in the same row with different superscript letters [a (highest values) – c (lowest values)] are significantly different at $p < 0.05$. Data are presented as mean ± SEM (n = 7/group).

References

Abdellatif, K.R.A., Fadaly, W.A.A., Kamel, G.M., Elshaier, Y.A.M.M., El-Magd, M.A., 2019. Design, synthesis, modeling studies and biological evaluation of thiazolidine derivatives containing pyrazole core as potential anti-diabetic PPAR-γ agonists and anti-inflammatory COX-2 selective inhibitors. Bioorganic Chemistry 82, 86-99.

Badawy, A., Hassanean, H., Ibrahim, A.K., Habib, E.S., El- Magd, M.A., Ahmed, S.A., 2019. Isolates From Thymelaea Hirsuta Inhibit Progression Of Hepatocellular Carcinoma In Vitro And In Vivo. Natural Product Research, DOI.10.1080/14786419.2019.1643859.

Chiappini, I., Fardella, G., Menghini, A., Rossi, C., 1982. Flavonoids from Dittrichia viscosa. Planta Med., 44, 159-166.

Elgazar, A.A., Selim, N.M., Abdel-Hamid, N.M., El-Magd, M.A., El Hefnawy, H.M., 2018. Isolates from Alpinia officinarum Hance attenuate LPS induced inflammation in HepG2: Evidence from In Silico and In Vitro Studies. Phytotherapy Research 32, 1273-1288.

El-Magd, M.A., Khalifa, S.F., A. Alzahrani, F.A., Badawy, A.A., El-Shetry, E.S., Dawood, L.M., Alruwaili, M.M., Alrawaili, H.A., Risha, E.F., El-Taweel, F.M., Marei, H.E., 2018. Incensole acetate prevents beta-amyloid-induced neurotoxicity in human olfactory bulb neural stem cells. Biomedicine & Pharmacotherapy 105, 813-823.

Horie, T., Ohtsuru, Y., Shibata, K., Yamashita, K., Tsukayama, M., Kawamura, Y., 1998. 13C NMR spectral assignment of the A-ring of polyoxygenated flavones. Phytochemistry 47, 865-874.

Llorensa, O., Pereza, Juan, J., Palomerc, A., Mauleonb, D., 2002. Differential binding mode of diverse cyclooxygenase inhibitors. J. Mol. Graph. Mod 20, 359-371.

Orlando, B.J., Malkowski, M.G., 2016. Substrate-selective inhibition of cyclooxygenase-2 by Fenamic Acid Derivatives Is Dependent on Peroxide Tone. J.Biol.Chem 291, 15069-15081.

Sanchez-Munoz, F., Dominguez-Lopez, A., Yamamoto-Furusho, J.K., 2008. Role of cytokines in inflammatory bowel disease. World J. Gastroenterol 14, 4280-4288.

Selim, N.M., Elgazar, A.A., Abdel-Hamid, N.M., El-Magd, M.R.A., Yasri, A., Hefnawy, H.M.E., Sobeh, M., 2019. Chrysophanol, Physcion, Hesperidin and Curcumin Modulate the Gene Expression of Pro-Inflammatory Mediators Induced by LPS in HepG2: In Silico and Molecular Studies. Antioxidants 8, 371.

Triantafilou, M., Triantafilou, K., 2005. Invited review: The dynamics of LPS recognition: Complex orchestration of multiple receptors. J. Endotoxin Res 11, 5-11.

Wang, X., Li, Y., Yang, X., Yao, J., 2013. Astragalus polysaccharide reduces inflammatory response by decreasing permeability of LPS-infected Caco2 cells. Int. J. Biol. Macromol 61, 347-352.

Yang H.S., Haj F.G., Lee M., Kang I., Zhang G., Lee Y., 2019. Laminaria japonica Extract Enhances Intestinal Barrier Function by Altering Inflammatory Response and Tight Junction-Related Protein in Lipopolysaccharide-Stimulated Caco-2 Cells. Nutrients 11(5):1001.